ISBN: 978-3-95450-232-5 ISSN: 2673-7000 doi:10.18429/JACoW-NAPAC2022-TUZE1

EXPERIMENTAL PHASE-SPACE TRACKING OF A SINGLE ELECTRON IN A STORAGE RING*

A. Romanov†, J. Santucci, G. Stancari, A. Valishev
Fermi National Accelerator Laboratory, Batavia, IL, USA

Abstract

This paper presents the results of the first ever experimental tracking of the betatron and synchrotron phases for a single electron in Fermilab's IOTA ring. The reported technology makes it is possible to fully track a single electron in a storage ring, which requires tracking of amplitudes and phases for both, slow synchrotron and fast betatron oscillations.

INTRODUCTION

Complete tracking of a charged particle in a circular accelerator will enable a new class of diagnostics capabilities. It will allow measurements of important single-particle dynamical properties, including dynamical invariants, amplitude-dependent oscillation frequencies, and chaotic behavior. The true single-particle measurements can be employed for benchmarking of long-term tracking simulations, for training of AI/ML algorithms, and ultimately for precise predictions of dynamics in present and future accelerators.

Observation of a single electron in storage rings has a long history that goes back to experiments at AdA, the first electron-positron collider [1, 2]. Several experiments using various instruments were done in the past to track single electron dynamics in storage rings, with the goal to track relatively slow synchrotron oscillations [3–5] and tracking of all 3 mode amplitudes [6].

If combined, state-of-the-art methods allow tracking of 4 dynamical variables out of 6 necessary to fully characterize particle motion in an accelerator. This study shows that it is possible to track betatron phases of a single particle in a storage ring with non-destructive measurements. There are two critical aspects that enable betatron phase tracking and that define its precision: the first is the quality of the measurements of the electron's coordinates; the second is the duration of the coherent betatron oscillations.

The described experiment, Betatron Oscillations Phase Tracking of a Single Electron (BOPTSE), helped define equipment parameters necessary for the full 6D tracking of a single electron in the IOTA ring by tracking a betatron phase in one plane [7].

EXPERIMENTAL METHOD

A straight-edge screen was placed in the focal plane of the synchrotron radiation imaging system at the M3L station to block photons from one of the halves of the phase space (as shown in Fig. 1). The vertical orientation of the screen was used for tracking a phase of the horizontal betatron oscillations. The measured counting rate of the M3L photomultiplier (PMT) with no obstruction is 7.5 kHz. To place the screen in the middle of the beam image, its position was adjusted until the counting rate reached 50% of the base rate. Coherent betatron oscillations over 50 ms (about 4×10^5 turns), with about 200 detected photons from one half of the phase space will allow precise reconstruction of phase and tune of the betatron oscillations. Analysis of longer data streaks will provide information about statistical properties and coherence of the betatron phase of a single electron.

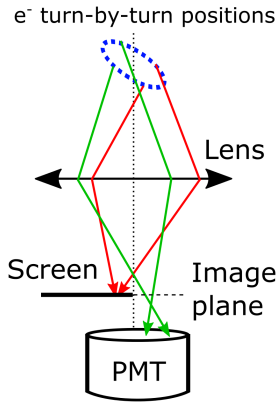

Figure 1: Optical scheme for betatron phase detection with shaded PMT.

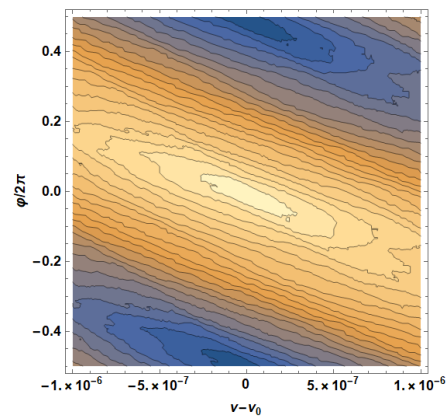

Figure 2: Contour plot of the correlation sum between simulated photons counts at PMT and model predictions for electron's position at corresponding turns depending on tune and phase of the betatron oscillations.

* This work was supported by the U.S. National Science Foundation under award PHY-1549132, the Center for Bright Beams. Fermi Research Alliance, LLC operates Fermilab under Contract DE-AC02-07CH11359 with the US Department of Energy.
† aromanov@fnal.gov

ISBN: 978-3-95450-232-5 ISSN: 2673-7000 doi:10.18429/JACoW-NAPAC2022-TUZE1

A simple simulation with a pure sinusoidal oscillator that randomly emits photons was done for a quick check of the proposed method. The rate of photons at the shadowed PMT was set to 3.75 kHz and 4×10^5 turns were simulated. Figure 2 shows a contour plot of a target function depending on phase ϕ and tune ν, $F(\phi, \nu)$:

$$F(\varphi_{x0}, \nu_x) = \sum_{i_\gamma} H\left[\sin(\varphi_x)\right] = \\ = \sum_{i_\gamma} H\left[\sin(2\pi(i_\gamma \nu + \varphi_{x0}))\right], \quad (1)$$

where $H(x)$ is the Heaviside step function and the summation is over all turn indices i_γ when photons were recorded.

The root mean square spread of the reconstructed phases and tunes after 30 simulations were $0.02 \times 2\pi$ and 7×10^{-8}, respectively. The exceptional precision of the reconstructed betatron tune is explained by the duration of the coherent oscillations, whereas the relatively small number of observations (about 200 photons) is not as relevant. This precision would allow us to study the statistical properties of the betatron phase. Another interesting aspect that can be studied is the amplitude dependence of the betatron tunes. The latter will require recording sets of images synchronized with data from the PMTs, to track slowly changing amplitudes.

When the horizontal plane is studied, information about synchrotron oscillations is helpful because of the coupling between longitudinal and horizontal planes through dispersion and chromaticity of the betatron oscillations. This information was extracted from the timing of the recorded photons.

Slow synchrotron oscillations introduce perturbations that can change the betatron phase by more than π, significantly reducing the available extent of the accurate coordinate predictions provided by the harmonic oscillator model. To the first order, the dependence of the betatron tune ν_x on the relative momentum deviation of an electron can be presented as:

$$\nu_x = \nu_{x0} + C_x A_p \sin(2\pi \nu_s n + \varphi_{s0}), \quad (2)$$

where C_x is the horizontal chromaticity, A_p is the amplitude of synchrotron oscillations in terms of relative momentum deviation, ν_s and φ_{s0} are the synchrotron tune and initial phase, and n is the turn number. Assuming $\nu_s \ll 1$, this expression can be integrated to get a betatron phase at a given turn n:

$$\frac{\varphi_x}{2\pi} = \nu_{x0} n + \frac{C_x A_t}{\alpha_p T_0}(\cos(\varphi_{s0}) - \cos(2\pi \nu_s n + \varphi_{s0})) + \frac{\varphi_{x0}}{2\pi}, \quad (3)$$

where α_p is the momentum compaction factor, T_0 is the revolution period and the amplitude of relative momentum deviation was expressed through the amplitude of relative time of arrival A_t:

$$A_p = \frac{2\pi \nu_s A_t}{\alpha_p T_0}. \quad (4)$$

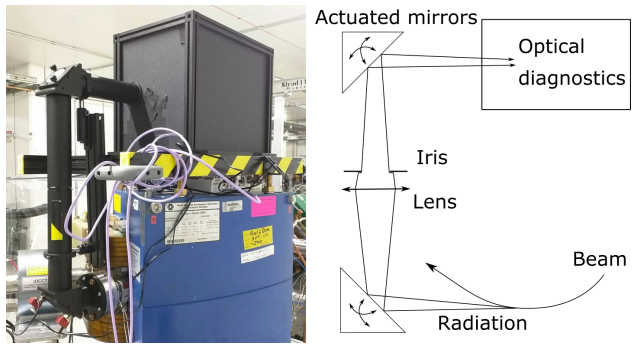

Figure 3: Photograph of the optical diagnostics setup at on of the IOTA's main dipoles (left) and corresponding schematic diagram (right).

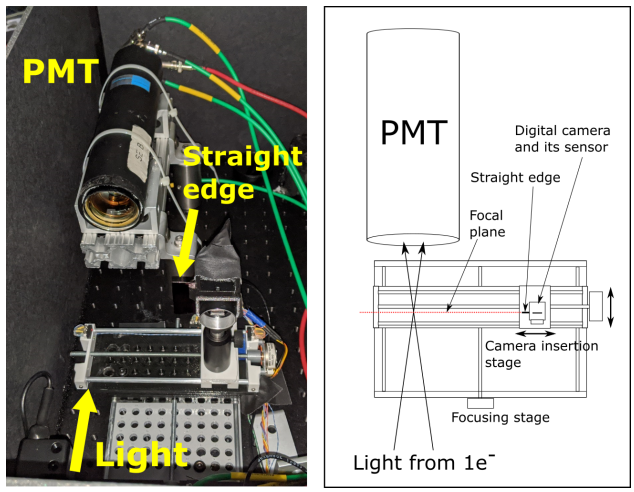

Figure 4: Photograph of the optical diagnostics setup for the BOPTSE experiment (left) and corresponding schematic diagram (right).

EXPERIMENTAL SETUP

Optical Diagnostics

Each of the 8 main dipoles in IOTA is equipped with synchrotron light stations installed on top of the magnets themselves. The light out of the dipoles is deflected upwards and back to the horizontal plane with two 90-degree mirrors. After the second mirror, the light enters the dark box, which is instrumented with customizable diagnostics, as shown in Fig. 3. Custom 3D-printed viewport adapters, 2-inch black tubes, and black fabric wrap were used to connect optical components and ensure light tightness. A focusing achromatic lens with a 40 cm focal length and an iris are installed in the vertical insulation tube that connects to the mirror holders. This experiment used 3 optical diagnostics stages equipped with sensitive digital cameras and one stage with shaded PMT.

The configuration of the M3L diagnostics box is presented in Fig. 4. The camera was located on stacked linear stages that can move it along the optical axis of the system and perpendicular to it. Movement along the optical axis allows

ISBN: 978-3-95450-232-5 ISSN: 2673-7000 doi:10.18429/JACoW-NAPAC2022-TUZE1

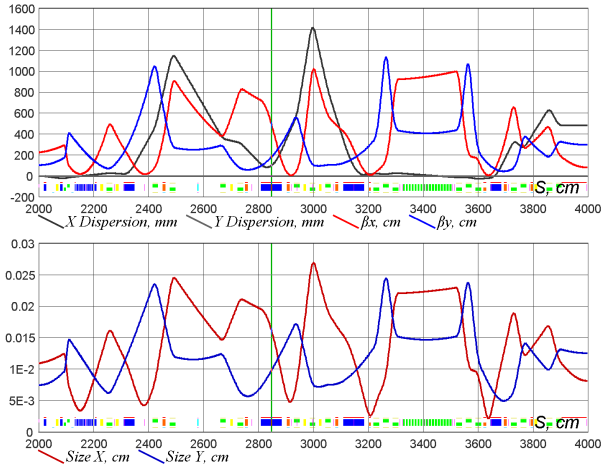

Figure 5: (top) Beta functions and horizontal dispersion of the BOTSE IOTA lattice.The second half of the ring is shown, ending at the injection straight section. (bottom) Beam sizes with 5.3 nm emittances in both planes for the lattice. The vertical green line shows location of the M3L monitor.

to put the camera's sensor in the focal plane and perpendicular movement can move the camera out of the light path to allow the necessary part of photons to reach PMT that is located behind the camera. A simple 3D-printed adapter attached to the digital camera was used to hold the straight vertical edge. This adapter positioned the knife-edge in the same plane as the sensor of the M3L camera. Transverse movement of the camera was used for rough positioning of the straight edge and fine control of the top actuated mirror was used to precisely block half of the phase space centered at projection of the equilibrium closed orbit.

IOTA Configuration

The conducted experiment required the IOTA ring configuration capable to sustain circulating beams with a lifetime longer than 100 s in a low-current mode. A special BOPTSE lattice was developed with relatively large emittances and long damping times for easier beam spot alignment and longer coherence of betatron oscillations. The main lattice parameters are listed in Table 1. The dispersion was minimized in the low-aperture regions of the ring. Polarities of all quadrupoles remained the same as used by the concurrent experiments. Figure 5 shows betatron functions, dispersion, and beam sizes for horizontal and vertical emittances of 5.3 nm.

The BOPTSE lattice was characterized using LOCO technique. The following tolerances are expected for the points of observation of the optical instruments:

- Beta functions accuracy of 10%
- Dispersion functions error smaller than 4 cm
- Phase advances within $0.01 \times (2\pi)$
- Betatron tunes within 0.001

Table 1: IOTA Parameters for BOPTSE Experiment

Parameter	Value
Perimeter	39.96 m
Momentum	101 MeV/c
Bunch intensity	$1 - 1000\ e^-$
RF frequency	30 MHz
RF voltage	55 V
Betatron tunes, (ν_x, ν_y)	(5.41, 3.44)
Synchrotron tune, ν_s	7.18×10^{-5}
Damping times, (τ_x, τ_y, τ_s)	(2.34, 2.04, 0.96) s
Horizontal emittance, ϵ_x	11.3 nm
Momentum spread, $\Delta p/p$, RMS	9.7×10^{-5}
Momentum compaction, α_p	0.015
Natural chromaticity C_x, C_y	-13.4, -9.0

RESULTS

Measured Data

To assist the offline analysis following calibration data has been taken:

- Calibration of the transverse linear stage that moves camera with the attached straight edge. The same type of linear stages is used for the focusing of the image by camera translation.
- Calibration of horizontal and vertical actuators on the last periscope's mirror.
- Calibration of the PMT counting rate for a wide range of beam intensities, down to a single electron and background rates.
- Turn-by-turn coordinates of a kicked beam at 100-150 µA using electrostatic pickups. Several combinations of kicks' amplitudes in X and Y plane were used.

The following data was collected with the IOTA synchrotron-light event timer and digital cameras:

- Turn numbers of photons detections.
- Photomultiplier signal arrival time with respect to the IOTA revolution marker, with an accuracy of about 15 ps. The resolution of the photomultiplier itself was on the order of 1 ns.
- Images from 3 digital cameras. The triggers were synchronized between cameras with about 2 ms, but relative synchronization with PMT data was not available. Absolute synchronisation could be done by alignment of independently reconstructed oscillations amplitudes.

Data sets for various straight edge positions were recorded. It could be used to reconstruct horizontal amplitude independently of digital cameras since the PMT's counting rate in the case of the off-central position of the straight edge depends on the electron's oscillations amplitude. For each position of the straight edge, several data streaks were recorded with

ISBN: 978-3-95450-232-5 ISSN: 2673-7000 doi:10.18429/JACoW-NAPAC2022-TUZE1

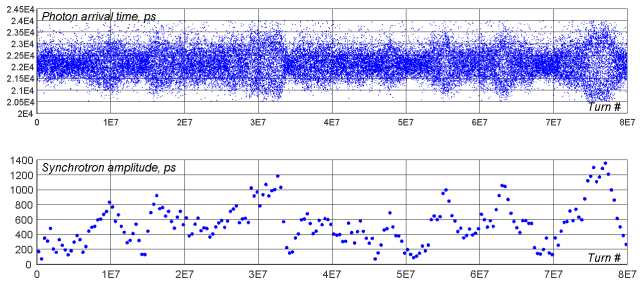

Figure 6: (top) Raw data from the M3L PMT timed photon detector over the first $8 \cdot 10^7$ turns, or about 10.7 seconds. (bottom) Reconstructed synchrotron oscillations amplitudes over the same time period.

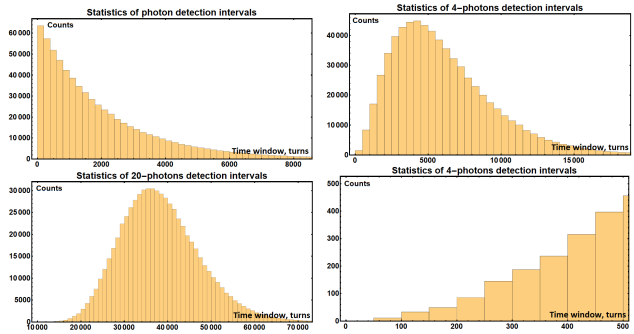

Figure 7: Distributions of number of turns that separate N^{th} detected photon and $(N+k)^{\text{th}}$ photon for all possible values of N. Top left histogram is for $k = 2$, or simply a distribution of photon's detection intervals; bottom left is a histogram for $k = 20$; top right is histogram for $k = 4$ and bottom right is the same case of $k = 4$ zoomed to show the distribution of the quickest series of 4 photons.

durations of 3 s, 10 s, and 180 s. Several 10 s streaks were recorded with horizontal kick triggered manually around 2-3 seconds after the start of the recording.

Injection of the beam into IOTA requires a transition to and from special injection configuration, which could lead to a small variation of the closed orbit due to the magnet's hysteresis. Therefore, every time an electron was lost and a new electron was captured in the ring with nominal lattice configuration, a verification of the straight edge position was done.

Reconstructing Synchrotron Oscillations

Chromatic effects must be accounted to track an electron over periods that are longer than a small fraction of synchrotron oscillations' period, which was about 14000 turns. Therefore the first step in the betatron oscillations tracking is a reconstruction of the synchrotron oscillations. For that, available data was split into sections of $4 \cdot 10^5$ turns and each section was used to determine the amplitude and phase of synchrotron oscillations.

Figure 6 shows photon arrival times for the first 10 seconds along with reconstructed amplitudes of synchrotron oscillations.

Statistical Properties of the Photons Detection

The distribution of time intervals between detected photons is compatible with the random nature of the radiation process and follows the exponential distribution. Natural fluctuations of the photons detection frequency can be used to select more favorable time intervals for the data analysis. The more photons are detected within a certain time interval, the higher precision of the reconstructed parameters would be. Figure 7 shows distributions of the time intervals containing certain number of detected photons.

Detecting Signal from Betatron Oscillations

As it was shown, the analysis method is highly sensitive to the betatron tune. The only known method to find the exact tune from the collected data is a brute-force search in the 2D parameter space of the betatron phase and tune. The best initial guess on the actual betatron tune was obtained from turn-by-turn coordinates from electrostatic pickups of a kicked macroscopic beam, which has a systematic error and statistical error of about $2 \cdot 10^{-4}$.

To decrease the complexity of the initial signal detection, a reduced number of photons was used over shorter time frames. This approach lowers the precision of the reconstructed values but significantly simplifies the initial search. Another advantage of the smaller numbers of photons in one streak is the possibility to pick a few sequences with a much more frequent detection rate compared to average, because of the random nature of the photon emission and detection processes. For example, in the analyzed data, there were 299 non-overlapping photon sequences with 4 photons detected within 300 turns. Such a short sequence doesn't allow to reconstruct the betatron phase, but averaging of the likelihood functions reveals a clear signal and approximate value of the betatron tune. A time window that is much shorter than the synchrotron oscillations period allows seeing signal even without accounting for the synchrotron oscillations (as presented in Fig. 8).

The most precise reconstruction of betatron frequency was obtained using data streaks of 40 photons detected within 60000 turns. The total number of analysed samples was 2000. Resulting spread of the betatron tune could be explained by several factors, for example:

- Fluctuations of power supplies of quadrupoles
- Dependence of the betatron tune on betatron amplitude of a single electron, which fluctuates due to random kickbacks from emitted photons and interactions with residual gas
- Nonlinear perturbations

As part of the BOPTSE lattice characterization effort, a series of turn-by-turn coordinates were measured after a macroscopic beam was kicked to various amplitudes in X and/or Y planes. All available electrostatic pickups were used to collect data. It was used to get initial guess for the betatron tune search and to verify the chromaticity of the

ISBN: 978-3-95450-232-5 ISSN: 2673-7000 doi:10.18429/JACoW-NAPAC2022-TUZE1

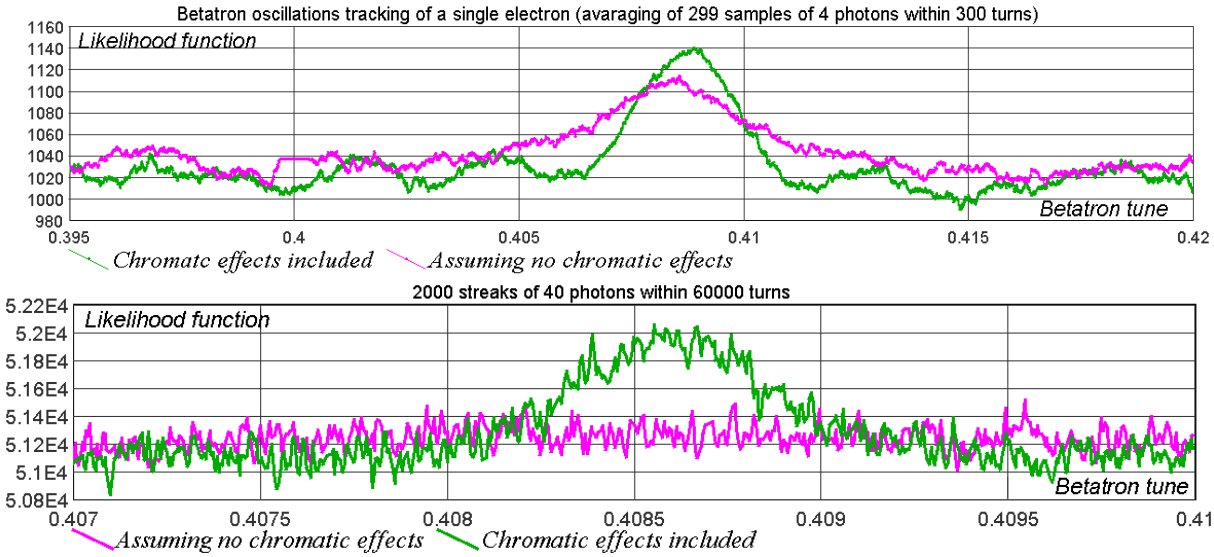

Figure 8: Sum of the likelihood functions for streaks of 4 photons detected within 300 turns with 299 streaks total (top), and 40 photons detected within 60000 turns with 2000 streaks total (bottom). Note the horizontal scale difference. The green line shows the sum with chromatic effects taken into account, the magenta line shows the less prominent peak in the case of a simple model of pure harmonic oscillations.

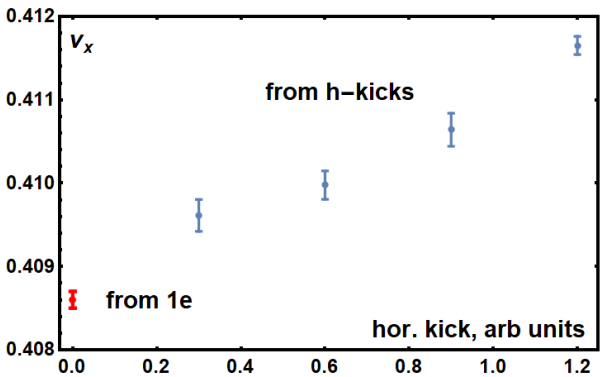

Figure 9: Horizontal betatron tune in the BOPTSE lattice obtained from analysis of turn-by-turn data after kicks with various amplitudes (blue dots). The same tune obtained from a single electron data without kicks is also shown for comparison (red dot).

lattice. One of the unexpected results is a relatively large difference between betatron tune measured with turn-by-turn data and with a single electron tracking (shown in Fig. 9).

SUMMARY

The BOPTSE experiment in combination with previous studies demonstrated the feasibility of a complete reconstraction of single electron trajectory in the 6D phase space.

Even readily available instruments with small additions allow precision measurements of true betatron tunes and chromaticities using a single particle.

With the addition of data from sensitive digital cameras, precise information about the amplitude dependence of betatron tunes can be measured.

Position sensitive photon detectors will enable even deeper analysis and understanding of storage rings, which is crucial for the successful design, commissioning, and operation of future accelerators.

ACKNOWLEDGEMENTS

We would like to thank the entire FAST/IOTA team at Fermilab for making these experiments possible, in particular D. Broemmelsiek, K. Carlson, N. Eddy, D. Edstrom, D. Franck, M. Obrycki, J. Ruan, and A. Warner.

REFERENCES

[1] C. Bernardini, "AdA: The first electron-positron collider," *Physics in Perspective*, vol. 6, no. 2, pp. 156–183, 2004. doi:10.1007/s00016-003-0202-y

[2] L. Bonolis and G. Pancheri, "Bruno Touschek and AdA: From Frascati to Orsay. in memory of Bruno Touschek, who passed away 40 years ago, on May 25th, 1978," INFN, Tech. Rep. 18-05/LNF, 2018.

[3] I. V. Pinayev, V. M. Popik, T. V. Shaftan, A. S. Sokolov, N. A. Vinokurov, and P. V. Vorobyov, "Experiments with undulator radiation of a single electron," *Nucl. Instrum. Methods Phys. Res. A*, vol. 341, no. 1, pp. 17–20, 1994. doi:10.1016/0168-9002(94)90308-5

[4] A. N. Aleshaev *et al.*, "A study of the influence of synchrotron radiation quantum fluctuations on the synchrotron oscillations of a single electron using undulator radiation," *Nucl. Instrum. Methods Phys. Res. A*, vol. 359, no. 1, pp. 80–84, 1995. doi:10.1016/0168-9002(96)88028-4

[5] I. V. Pinayev *et al.*, "A study of the influence of the stochastic process on the synchrotron oscillations of a single electron

ISBN: 978-3-95450-232-5 ISSN: 2673-7000 doi:10.18429/JACoW-NAPAC2022-TUZE1

circulated in the VEPP-3 storage ring," *Nucl. Instrum. Methods Phys. Res. A*, vol. 375, no. 1, pp. 71–73, 1996. doi:10.1016/0168-9002(95)01350-4

[6] A. Romanov, J. Santucci, G. Stancari, A. Valishev, and N. Kuklev, "Experimental 3-dimensional tracking of the dynamics of a single electron in the fermilab integrable optics test accelerator (IOTA)," *JINST*, vol. 16, no. 12, P12009, 2021. doi:10.1088/1748-0221/16/12/p12009

[7] S. Antipov *et al.*, "IOTA (Integrable Optics Test Accelerator): Facility and experimental beam physics program," *JINST*, vol. 12, no. 03, T03002–T03002, 2017. doi:10.1088/1748-0221/12/03/t03002